Materials & Design 236 (2023) 112467

Contents lists available at ScienceDirect

Materials & Design

journal homepage: www.elsevier.com/locate/matdes

Soft composite actuators of poly(vinylidene fluoride-trifluoroethylene-chlorotrifluoroethylene)-based nanofibers and polydimethylsiloxane: Fabrication, electromechanical characterization, and dynamic modeling

Riccardo D'Anniballe [a,*], Giacomo Selleri [b], Leon Wierenga [a], Andrea Zucchelli [c], Davide Fabiani [b], Raffaella Carloni [a]

[a] Bernoulli Institute for Mathematics, Computer Science and Artificial Intelligence, Faculty of Science and Engineering, University of Groningen, Nijenborgh 9, 9747 AG Groningen, the Netherlands
[b] Department of Electrical, Electronics and Information Engineering "Guglielmo Marconi", University of Bologna, Viale del Risorgimento 2, 40136 Bologna, Italy
[c] Interdepartmental Centre for Industrial Research in Advanced Mechanical Engineering Applications and Materials Technology, Department of Industrial Engineering, University of Bologna, Viale Risorgimento 2, 40136 Bologna, Italy

ARTICLE INFO

Keywords:
Soft actuators
P(VDF-TrFE-CTFE)
Electrospun nanofibers
Fiber composite

ABSTRACT

Nanofibrous unimorph cantilever beam soft actuators offer remarkable advantages, such as rapid viscoelastic relaxation, low power consumption, and high weight-specific properties. However, the presence of high porosity in the nanofibrous active layer poses a challenge due to its low breakdown voltage, limiting the practical applications of this class of soft actuators. This study proposes an innovative solution to enhance the relative permittivity of the nanofibrous layer by redesigning it as a composite layer. By integrating electrospun aligned nanofibers of poly(vinylidene fluoride-trifluoroethylene-chlorotrifluoroethylene) into a polydimethylsiloxane elastomeric matrix, the composite active layer achieves a notable increase in relative permittivity (10.5 at 100 Hz), surpassing the individual materials' values (2.5 and 2.7 at 100 Hz for the nanofibers and polydimethylsiloxane, respectively). To realize novel soft actuators, the composite active layer is placed between carbon black electrodes, with Kapton® serving as the passive layer. Remarkably, aligning the nanofibers in the transversal direction of the actuator enhances its actuation capabilities significantly. When subjected to a 25 MVm^{-1} electric field, the tip deflection and blocking force exhibit a ~400% improvement compared to polydimethylsiloxane-based actuators. To support these findings, a physics-based dynamic model is derived and validated through experimental tests in both static and transient time simulations.

1. Introduction

The poly(vinylidene fluoride-trifluoroethylene-chlorotrifluoroethylene), commonly referred to as P(VDF-TrFE-CTFE), is a relaxor ferroelectric polymer known for its electrostrictive strain characteristics. It possesses the remarkable ability to generate a substantial field-induced strain when subjected to an external electric field. Given this distinctive property, the scientific community has shown a growing fascination with employing this polymer in the burgeoning field of soft robotics [1–4].

Previous work has introduced and examined soft actuators constructed as unimorph cantilever beams, employing two distinct morphologies for the active layer: an extruded film and a mat of aligned electrospun nanofibers of P(VDF-TrFE-CTFE) [5]. This investigation has demonstrated that the nanofibers-based soft actuator, in comparison to the film-based counterpart, showcases superior characteristics such as faster viscoelastic relaxation, reduced power consumption, and enhanced weight-specific properties. Despite these advancements, the persistently challenging issue revolves around the high porosity of the nanofibrous structure and its consequential impact on the low break-

* Corresponding author.
E-mail address: r.danniballe@rug.nl (R. D'Anniballe).

https://doi.org/10.1016/j.matdes.2023.112467
Received 30 May 2023; Received in revised form 1 November 2023; Accepted 5 November 2023
Available online 10 November 2023

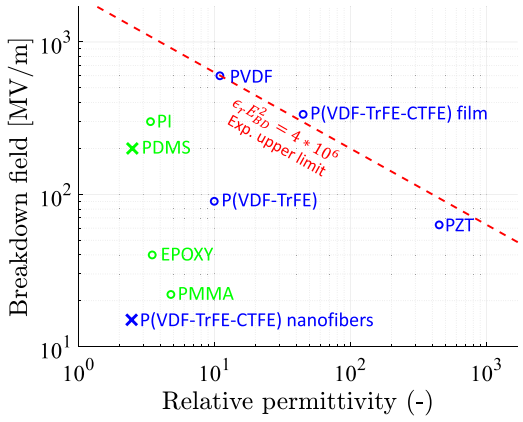

Fig. 1. Breakdown voltage versus relative permittivity for selected ferroelectric polymeric and ceramic materials, as retrieved from [16], from [17] and [18] for the PZT, from [19] for the PVDF, from [20] and [21] for the PVDF-TrFE.

down field of the active layer in these electrostrictive actuators. This limitation poses a significant hurdle, hindering the practical realization of nanofibrous electrostrictive actuators that necessitate the high electric fields to be activated.

This study proposes a novel approach to address the challenge posed by the high porosity of nanofibrous mats in electrostrictive materials like the P(VDF-TrFE-CTFE). The solution involves seamlessly integrating these electrospun nanofibrous mats into a soft elastomeric matrix, effectively eliminating the air gaps between the fibers. It is worth noting that this integration process has already been successfully employed in other domains of application, such as the development of soft sensors [6–8], high performance fiber reinforced composites [9–11], and batteries [12–14]. Leveraging this well-established technique, the limitations associated with high porosity can be overcome and the full potential of electrostrictive actuators in the realm of soft robotics can be unlocked.

An appropriate polymeric matrix for the integration of nanofibers can be found by analyzing the total strain η induced in an electrostrictive polymeric material upon the application of an electric field E [15], i.e.:

$$\eta = \eta^{Maxwell} + \eta^{electrostriction} = -\frac{1}{2}\frac{\epsilon_0 \epsilon_r E^2(1+2\nu)}{Y} + Q P'^2 \quad (1)$$

which is given by the sum of the Maxwell stress (as a function of the polymer Young's modulus Y, the polymer Poisson's coefficient ν, the polymer relative permittivity ϵ_r, the vacuum permittivity ϵ_0) and of the electrostrictive effect (as a function of the electrostrictive coefficient Q and the phase transformation-induced polarization P' of the polymer). By analyzing Equation (1), it is clear that, to enhance the effect of the Maxwell stress, the polymeric matrix should maximize the ratio ϵ_r/Y between the relative permittivity and the Young modulus.

Fig. 1 classifies various ferroelectric polymers (in blue) and polymeric matrices (in green) that have been previously utilized in relevant literature for integrating nanofibers. This classification is based on the relative permittivity and breakdown field characteristics of these materials. Notably, the P(VDF-TrFE-CTFE) nanofibers, due to the presence of air gaps, are positioned in the bottom-left quadrant of the figure. By integrating the nanofibers into a suitable polymeric matrix, the gaps between the fibers can be effectively filled. This integration process leads to a significant improvement in both the breakdown strength and relative permittivity of the resulting composite material. Consequently, the composite achieves enhanced performance compared to the individual nanofibers, making it a compelling choice for advanced applications.

In this study, the polydimethylsiloxane (PDMS) is chosen as elastomeric matrix, primarily due to its desirable properties, including a low Young's modulus, stable electrical properties, and ease of moldability [7]. It is crucial to highlight that the composite active layer

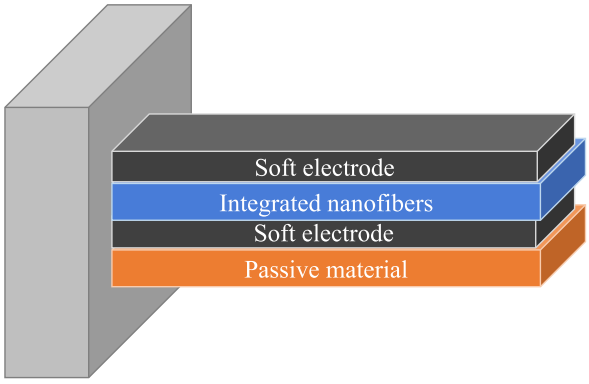

Fig. 2. The soft actuators as a composite unimorph cantilever beam.

Table 1
Dimensions (free length l, breadth b, thickness t) of the layers of the soft actuator.

Material	l [mm]	b [mm]	t [μm]
Composite layer	45	20	~60
Electrodes	43	18	~80
Kapton® tape	45	20	~57

for the soft actuators, purposefully designed as P(VDF-TrFE-CTFE)-based nanofibers integrated into PDMS, possesses intrinsic anisotropy attributed to the alignment of the nanofibers during the electrospinning process. This aligns this study with the current trends in the literature, which actively seeks anisotropic properties for the development of advanced soft actuators [22–24].

The remainder of the paper is organized as follows. Section 2 presents the fabrication and characterization of the P(VDF-TrFE-CTFE) electrospun nanofiber mat, the procedure needed for the integration in the PDMS silicone matrix, and the fabrication of composite unimorph cantilever beam soft actuators. Section 3 describes the electromechanical characterization of the fabricated soft actuators. Section 4 presents an electrical and mechanical analysis of the integrated nanofibers, and the physics-based model of the composite soft actuator, based on finite element analysis. Section 5 shows the results of the electromechanical characterization for the validation of the physics-based model. Section 6 discussed the properties of the actuator, evaluated by using the physics-based model. Finally, concluding remarks are drawn in Section 7.

2. Fabrication of the composite soft actuator

This Section describes the fabrication process of the soft actuator that has been designed as a composite unimorph cantilever beam [4, 25], and sketched in Fig. 2. The active layer is a composite of P(VDF-TrFE-CTFE) electrospun aligned nanofibers integrated in the PDMS silicone elastomer (Sylgard™ 184, Silicone elastomer kit) and it is interleaved between two conductive carbon black-based flexible electrodes. The passive layer is Kapton® tape, which is placed on one side creating an asymmetric structure and holding the complete soft actuator together. The dimensions of the different layers of the proposed soft actuator are reported in Table 1.

2.1. P(VDF-TrFE-CTFE) electrospun aligned nanofibers

The aligned nanofibers of P(VDF-TrFE-CTFE) have been realized by an electrospinning process. Specifically, for the fabrication of a mat of nanofibers, a solution of P(VDF-TrFE-CTFE) powder (30 wt%), provided by Solvay Specialty Polymers (Milano, Italy, www.solvay.com)) and Acetone:DMF 55:45 (w/w) is processed by an electrospinning machine (Spinbow™, Bologna, Italy, www.spinbow.it/en), equipped with two needles (length of 55 mm and internal diameter of 0.84 mm) that

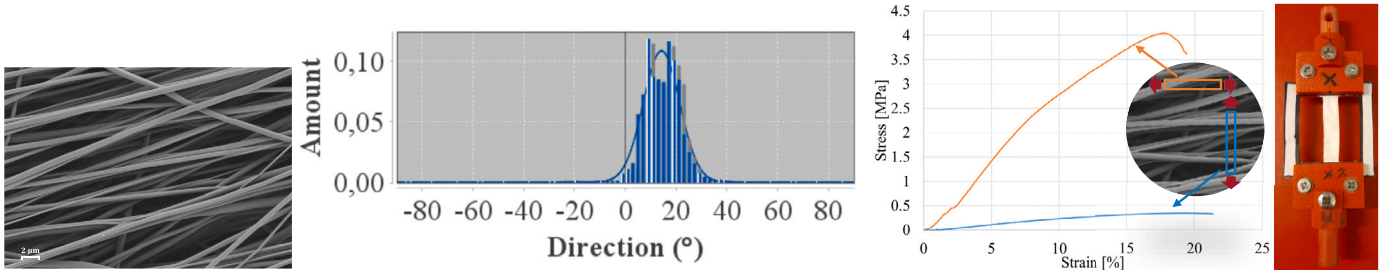

Fig. 3. (a) SEM image of one specimen of the aligned nanofibers mat. (b) Directionality histogram. (c) Specimen anchored in a paper frame, and tensile test results in the longitudinal and transverse direction with respect to the alignment direction of the nanofibers.

Table 2
Electrospinning parameters used for the production of the P(VDF-TrFE-CTFE) nanofiber mats.

Flow rate [ml/h]	0.55
Electric potential [kV]	16
Drum rotation speed [rpm]	6700
Distance needles-drum [cm]	16
Relative humidity [%]	23
Temperature [°C]	21

are connected to 5 mL syringes via PTFE tubings. The nanofibers have been collected on a rotating drum, covered with poly(ethylene)-coated paper. The parameters of the electrospinning process are summarized in Table 2.

Fig. 3a reports an image of a portion of the mat of the P(VDF-TrFE-CTFE) nanofibers, obtained with a Supra 55 scanning electron microscope (SEM) (Zeiss, Germany, www.zeiss.com), which shows the aligned nanofibers. To quantify the alignment of the fibers, the SEM image was analyzed with the ImageJ software, with the Directionality plugin (www.imagej.net) [26]. The directionality histogram in Fig. 3b reports the amount of fibers as a function of the fiber orientation, showing that the majority of the fibers are oriented on a preferential direction.

The Young's modulus of the aligned nanofibers has been evaluated in tensile tests with the test instrument ElectroPuls E1000 (Instron™, Norwood (MA), USA, www.instron.us), which is equipped with a 5 N Instron™ static load cell 2530-5N. A specimen is placed in the test instrument by following a well established procedure to avoid any damage to the nanofibers [5]. Firstly, the specimen is anchored into a paper frame with a bi-adhesive tape to prevent slippage. Then, the paper frame is clamped by means of two 3D-printed ABS clamps in the test instrument (see Fig. 3c) and, finally, the paper frame is cut on the sides, leaving the specimen properly placed in the test instrument.

The Young's modulus of the aligned nanofiber is evaluated longitudinally and transversally with respect to the alignment direction of the nanofibers. Each tensile test has been repeated on at least three specimens, and the Young's modulus of each specimen is evaluated as the slope of the tangent to the stress-strain curve at low strain. Fig. 3c reports the results of a tensile test on a specimen, for which the average Young's modulus in the longitudinal direction (in orange) is 50 MPa, with a standard deviation of 5.40 MPa, while the average Young's modulus in the transverse direction (in blue) is 4 MPa, with standard deviation of 0.4 MPa. Due to the difference between these two Young's moduli, it is possible to conclude that the mat of P(VDF-TrFE-CTFE) electrospun aligned nanofibers is intrinsically anisotropic.

2.2. Integration of the P(VDF-TrFE-CTFE) nanofibers in the PDMS silicone elastomer

Specimens have been cut from the mat of P(VDF-TrFE-CTFE) nanofibers and have been integrated into a matrix of PDMS silicone elastomer.

The integration process is sketched in Fig. 4. Firstly, the PDMS is mixed with the curing agent (weight ratio 10:1) and the resulting solution is placed into a vacuum chamber to remove air bubbles. Afterwards, the PDMS is deposited on the specimen of nanofibers, lying on a teflon substrate, by means of a blade [7]. After a precuring phase in oven (10 min, 50 °C), a second blading on the specimen is performed to remove any excess of PDMS. The obtained composite layer is, finally, cured in oven at 90 °C for 1 h.

The two SEM images of the cross-section, as reported in Fig. 4, show the difference between two specimens before and after the second blading. Specifically, it is possible to appreciate an excess of PDMS on top of the composite layer (nanofibers integrated in PDMS), which is completely removed by the second blading. It is important to remove the excess of PDMS since it would decrease the electrical properties of the active layer of the soft actuator, as it will be further discussed in the next section.

2.3. Composite soft actuator

To preserve the flexibility of the composite active layer, soft electrodes are realized by dispersing conductive carbon black nanoparticles in the PDMS [27]. In particular, 17.5% wt of carbon nanoparticles (Super P, BET specific surface area of 62 ± 5.0 m^2/g, average particles size of 40 nm) are added to the PDMS. Then, the solution is prepared by adding 300% wt of isopropanol and by magnetically stirring for 1 h at room temperature. Next, the curing agent is added and, after mixing, the solution is placed into an oven at 40 °C for 12 min to allow the isopropanol to evaporate. By using a blade, a homogeneous layer is placed on the composite layer and cured for 1 h at 90 °C. The same process is repeated for the opposite electrode on the other side. The complete soft actuator is obtained by placing the fabricated structure on a layer of Kapton® tape that acts as a passive layer. Fig. 5 shows (a) the soft actuator, in both (b) rest state (no electric field is applied) and (c) bent state (an electric field is applied).

Three different types of soft actuators, which are built using the same passive kapton layer and carbon based electrodes but are differing only in the active layer, have been fabricated: (i) P(VDF-TrFE-CTFE)-based nanofibers integrated in PDMS aligned transversally to the actuator length; (ii) P(VDF-TrFE-CTFE)-based nanofibers integrated in PDMS aligned longitudinally to the actuator length; (iii) Only PDMS. The dimensions of the soft actuators are the same as reported in Table 1.

3. Electromechanical characterization methodology

This Section describes the experimental set-ups used for the electromechanical characterization of the soft actuators to analyze and measure the tip deflection and the blocking force.

3.1. Tip deflection

A digital AM7915MZT(L) 5 MPx microscope (Dino-Lite, AnMo Electronics Corp, Taipei, Taiwan, www.dino-lite.com) is used to record,

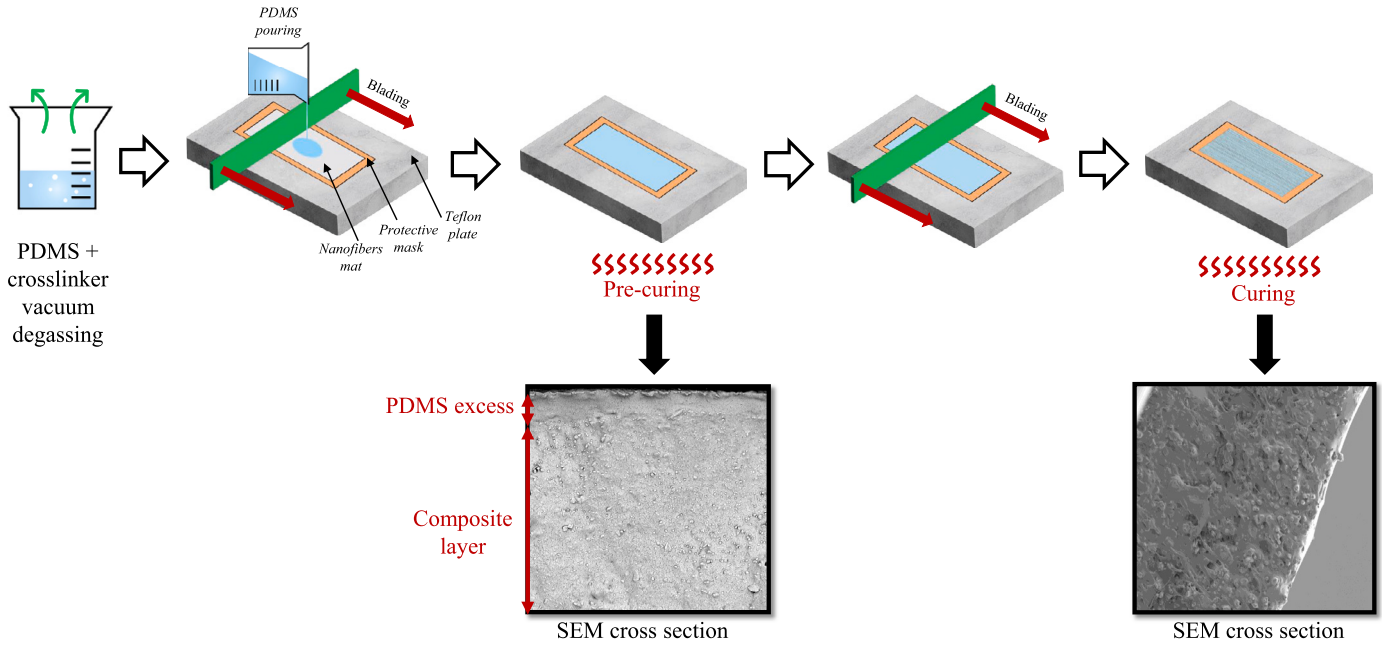

Fig. 4. Integration steps of the P(VDF-TrFE-CTFE)-based nanofibers into a PDMS silicone elastomer. The nanofibers mat is placed on a teflon substrate and integrated in PDMS after two subsequent blading and curing steps. The SEM images show the integrated nanofibers with and without an excess of PDMS (i.e., before and after the second blading).

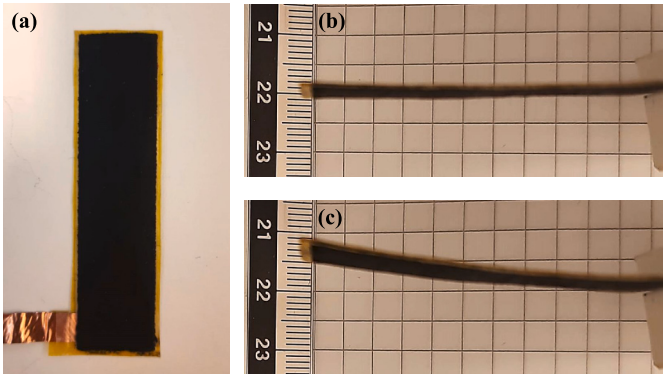

Fig. 5. (a) Top view of the soft actuator. (b) The soft actuator is at rest (no electric field is applied). (c) The soft actuator bends when an electric field is applied.

with a sample rate of 20 Hz, the deflection of the tip of the actuators when stimulated by DC and AC electric fields of varying frequency and magnitude. One extremity of the actuator is kept fixed by a support, designed and 3D printed in ABS material, while the other extremity is free to move. The deflection is recorded in a video with the DinoCapture software (version 2.0) which is, then, analyzed in Matlab (Mathworks, USA, https://www.mathworks.com). To measure the deflection of the actuators, a tracking algorithm of the tip of the actuator is used, as proposed in [28].

3.2. Blocking force

The test set-up consists of the test instrument Instron™ ElectroPuls E1000, equipped with a 5 N Instron™ static load cell 2530-5N and an optical encoder. A 10/10B-HS high-voltage amplifier (Trek Inc., Lockport, New York, USA, www.trekinc.com) is connected through crocodile plugs to the electrodes of the soft actuator and is operated through the DG1022 waveform generator (RIGOL Technologies, Beaverton, Oregon, USA, www.rigolna.com). The Instron™ Wavematrix software records both the forces measured by the load cell and the applied electric fields with a sample rate of 50 Hz. In the test instrument, the soft actuators are held at one extremity by a support, designed and 3D printed in ABS material, while the other extremity is in contact with the load cell that registers the exerted force.

4. Constitutive model of the soft actuator

This Section presents the physics-based electromechanical model of the soft actuator, whose composite active layer has been designed as P(VDF-TrFE-CTFE) electrospun aligned nanofibers integrated in the PDMS silicone elastomer. Alternatively to homogenization techniques, representing the fiber as volume element at the microscale [29], equivalent electrical and mechanical model of the composite layer are proposed in this work to determine the effective parameters.

Initially, the electrostrictive equations are mathematically formulated, highlighting key parameters for solving them. These parameters are determined through experiments, following modeling of the composite layer's electrical and mechanical aspects, and then they are used in the dynamic physics-based finite element model.

4.1. Constitutive equations of the composite active layer

Starting from the kinematics, a dielectric material in the initial stress-free state condition is denoted by Ω_0, and $\delta\Omega_0$ denotes its boundary [30–32]. Actuated by both mechanical and electrical stimuli, the material body deforms to the configuration Ω. One material point identified by its position vector X in Ω_0 can be mapped to the corresponding point identified by its new position vector x in Ω by the mapping function $x = \chi(X)$. The deformation gradient tensor F defined by:

$$F = \frac{\delta x}{\delta X} = \nabla \chi(X) \tag{2}$$

is introduced for the deformation measure.

To determine the deformation, Maxwell's equations need to be solved for the electrostatic fields, under the assumption that only electrostatics hold for the electromagnetic field [33]:

$$\nabla \cdot d = 0, \nabla \times e = 0 \tag{3}$$

where d is the electric displacement tensor, and e is the electric field respect to the deformed configuration. At the surfaces of discontinuity, including the boundary $\delta\Omega_0$, the electric field and the electric displacement must fulfill the jump conditions:

$$[\![d]\!] \cdot n = 0 \; and \; [\![e]\!] \times n = 0 \tag{4}$$

where brackets $[\![\bullet]\!]$ indicate a jump and where n is the outward unit normal to the surface of discontinuity.

The deformation of linear elastic materials subjected to external loads is described by Cauchy's balance equation:

$$\rho \frac{\delta u^2}{\delta t^2} = \nabla \cdot \sigma + f + f_e \tag{5}$$

where ρ is the density, u denotes the structural displacement vector, σ is the Cauchy stress tensor of elasticity, f is the body force, and f_e represents the electric body force.

In the stationary case and in the absence of body external forces the Equation (5) can be written as:

$$\nabla \cdot \sigma + f_e = 0 \tag{6}$$

The electric body force f_e, when employing Equation (3), can be written as the divergence of a second order tensor, namely:

$$f_e = \nabla \cdot \tau_e \tag{7}$$

where τ_e is the Maxwell stress tensor in free space and is defined as [34]:

$$\tau_e = d \otimes e - \frac{1}{2}(e \cdot e) I \tag{8}$$

where I is the second-order identity tensor; the relation between e and d is $d = \epsilon_0 e + p$, where ϵ_0 is the vacuum permittivity and p is the electric polarization. Let be τ the total stress tensor, defined by:

$$\tau = \sigma + \tau_e \tag{9}$$

so that the equilibrium Equation (6), becomes:

$$\nabla \cdot \tau = 0 \tag{10}$$

Specifically, the total stress τ takes the representation:

$$\tau = \sigma + d \otimes e - \frac{1}{2}(e \cdot e) I \tag{11}$$

Assuming a linear dielectric composite material with constant relative permittivity ϵ_c, obeying the constitutive relation:

$$d = \epsilon_0 \epsilon_c e \tag{12}$$

Equation (11) can be written as:

$$\tau = \sigma + \epsilon_0 \epsilon_c [e \otimes e - \frac{1}{2}(e \cdot e) I] \tag{13}$$

For a linear elastic material, Hooke's law relates the stress tensor σ to the elastic strain tensor η:

$$\sigma = C : \eta \tag{14}$$

where C is the 4^{th} order stiffness tensor, stands for the double-dot tensor product and the strain η is given by $\eta = \frac{1}{2}(\Delta u + \Delta u^T)$.

The direct electrostrictive effect [35–37] can be represented as an additive contribution to the elastic strain η:

$$\eta_{el} = Q : (p \otimes p) \tag{15}$$

Therefore, the stress tensor σ, in case of an electric field, can be augmented with η_{el} [38]:

$$\sigma = C : (\eta - \eta_{el}) \tag{16}$$

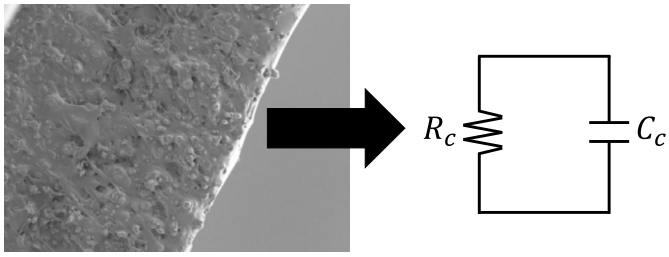

Fig. 6. SEM image of the composite active layer and its equivalent electric circuit.

Finally, the Equation (11), can be written as:

$$\tau = C : [\eta - Q : (p \otimes p)] + \epsilon_0 \epsilon_c [e \otimes e - \frac{1}{2}(e \cdot e) I] \tag{17}$$

The formulation of the equations discussed above is Eulerian in character in that the field variables e and p are defined in the deformed configuration as functions of the deformed position vector x. Their referential counterparts E and P can be defined through the transformations:

$$E = e \cdot F \; , \; P = p \cdot F \tag{18}$$

Finally, to build a physics-based finite element model (FEM) of the soft actuator, it is required to evaluate the total stress τ and, therefore according to Equations (17) and (18), it is required to measure the composite relative permittivity ϵ_c, the electric polarization P, and the stiffness tensor C.

4.2. Equivalent electrical model of the composite active layer

The composite active layer together with its equivalent electric circuit are shown in Fig. 6. The composite active layer can be modeled as the parallel of a resistor R_c (describing the current leakage through the layer) and of a capacitance C_c (describing the charge stored in the layer, i.e., a parallel-plate capacitor) [5].

4.2.1. Relative permittivity

To evaluate the relative permittivity of the composite active layer, it is possible to correlate the dielectric properties of the material with macroscopic parameters, such as the material porosity. Specifically, this study uses the Vegard approximation [39] as a simple mixing model correlating the relative permittivity ϵ_{model} of the composite material with the porosity P_{NF} of the nanofibrous mat through the relation:

$$\epsilon_{model} = P_{NF} \; \epsilon_{PDMS} + \left(1 - P_{NF}\right) \epsilon_{PVDF} \tag{19}$$

where ϵ_{PDMS} and ϵ_{PVDF} are the relative permittivities of the PDMS and of the P(VDF-TrFE-CTFE) bulk polymer, respectively.

The porosity of the nanofibers mat can be calculated as [40]:

$$P_{NF} = \left(1 - \frac{\rho_{NF}}{\rho_{PVDF}}\right) \cdot 100 \tag{20}$$

where ρ_{NF} is the density of the nanofiber mat and ρ_{PVDF} the density of the P(VDF-TrFE-CTFE) bulk polymer.

The capacitance of the composite layer C_c can be directly measured with a Voltcraft LCR-400 meter. From this measurement, it is possible to compute the relative permittivity ϵ_c of the composite active layer, i.e.:

$$\epsilon_c = \frac{C_c t_c}{A \epsilon_0} \tag{21}$$

where A is the active layer area, t_c the total thickness of the active layer, and ϵ_0 the vacuum permittivity.

However, when the integration of the nanofiber mat in PDMS is made without the pre-curing step, as described in Section 2.2, the active

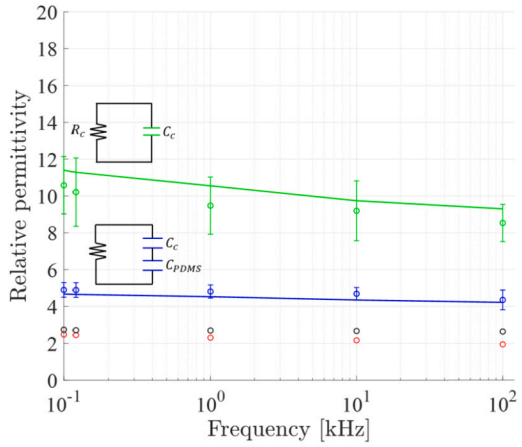

Fig. 7. Relative permittivity of the nanofibers mat alone (red), of the pure PDMS (black), of the nanofibers integrated in PDMS with an excess of PDMS (blue), and of the nanofibers integrated in PDMS (green) at different frequencies. The continuous lines correspond to the model results.

layer would be made of two consecutive layers, i.e., the layer with the nanofibers integrated in PDMS and the layer with the excess of PDMS. In this case, the equivalent electric circuit would be given by the parallel of a resistor and of a capacitance C_{eq}, given by the series of two capacitors (one for each layer), i.e.:

$$C_{eq} = \frac{1}{\frac{1}{C_c} + \frac{1}{C_{PDMS}}} \tag{22}$$

Where C_{PDMS}, is the capacitance of the layer in excess of PDMS.

By using the Vegard approximation, C_c can be also evaluated by using ϵ_{model} of Equation (19). Consequently, Equation (22) can be written as:

$$C_{eq} = \frac{1}{\frac{1}{\frac{\epsilon_{model} A \epsilon_0}{t_c}} + \frac{1}{\frac{\epsilon_{PDMS} A \epsilon_0}{t_{PDMS}}}} \tag{23}$$

where t_{PDMS} is the thickness of the PDMS layer in excess.

The modeled permittivity ϵ_{eq} for the two consecutive layers can be expressed as:

$$\epsilon_{eq} = \frac{C_{eq}\, t_{c+PDMS}}{A\, \epsilon_0} \tag{24}$$

where t_{c+PDMS} is the total thickness of the two consecutive layers.

Finally, to compare the modeled ϵ_{eq}, the experimental value of the capacitance of the two consecutive layers, denoted as C_{c+PDMS}, can be measured with the Voltcraft LCR-400 meter and the relative permittivity ϵ_{c+PDMS} of the two consecutive layers can be derived in analogy with Equation (21), i.e.:

$$\epsilon_{c+PDMS} = \frac{C_{c+PDMS}\, t_{c+PDMS}}{A\, \epsilon_0} \tag{25}$$

Fig. 7 shows, at different frequencies, the relative permittivity of the composite layer ϵ_c (in green, and derived from experimental data by using Equation (21)), the relative permittivity of the composite layer with excess of PDMS ϵ_{c+PDMS} (in blue, and derived from experimental data by using Equation (25)), the relative permittivity of the nanofibers mat alone (in red) [5], and the relative permittivity of the pure PDMS (in black). The continuous green and blue lines are the relative permittivity computed by using Equation (19) for the composite layer and Equation (24) for the composite layer with excess of PDMS, respectively, for which the average values of porosity $P_{NF} = 70$.

It is possible to notice that, as described by Equation (19), the integrated nanofibers have an higher relative permittivity compared to the pure PDMS and to the nanofibers mat alone, due to the air gaps filled with PDMS in the integrated fibers. When the excess of PDMS is removed with the pre-curing, the relative permittivity further increases. Specifically, at 100 Hz, the relative permittivity (average ± standard deviation) of the composite layer without excess of PDMS is 10.5, while the nanofibers mat and the pure PDMS have an average relative permittivity of 2.5 and 2.7, respectively. The Vegard model is validated as it interpolates the experimental data points at different frequencies.

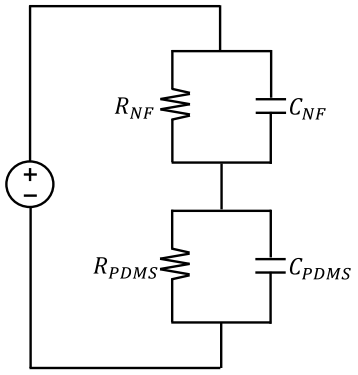

Fig. 8. Equivalent electrical circuit of the composite layer used for the derivation of the electric polarization.

4.2.2. Electric polarization

The polarization P, represents the electric polarization induced by a certain applied electric field, and obtained from displacement-electric field (D-E) loops [15]. When a dielectric material is placed in an electric field, it acquires a polarization that depends on the electric field E, given by the relation $P = \chi_e E$, where χ_e is the electric susceptibility. To find the electrostrictive contribution to the total strain due to the polarization of the active layer when an external electric field is applied, the equivalent electric circuit of Fig. 8 is used, which is represented by the series of the parallel of a capacitor and a resistance of the nanofibers and of the PDMS, i.e., (R_{NF}, C_{NF}) and (R_{PDMS}, C_{PDMS}), respectively.

When an electric field is applied to the integrated nanofibers, the electric field is distributed unevenly to the nanofibers and the embedding medium according to their electrical properties, unlike a bulk sample (such as a film) for which the electric field is applied directly to it. The amount of electric field E_{NF}, responsible for the electric polarization of the nanofibers, is given by [7]:

$$E_{NF} = \frac{\frac{E h_{tot}}{\sigma_{NF}}}{\frac{h_{NF}}{\sigma_{NF}} + \frac{h_{PDMS}}{\sigma_{PDMS}}} \tag{26}$$

where E is the applied electric field, σ_{NF} the electrical conductivity of the nanofibers, and h_{PDMS}, h_{NF}, h_{tot} the thickness of the embedding medium (the PDMS), of the nanofibers, and of the complete active layer, respectively.

For the produced specimens, the total thickness is $h_{tot} = 60$ μm, while the thickness of the nanofibers $h_{NF} = 18$ μm and of the PDMS $h_{PDMS} = 42$ μm are derived with a weighted percentage from the nanofibers porosity. The electrical conductivity of the nanofibers is $\sigma_{NF} = 3.10E^{-10}$ S/m [5], the conductivity of the PDMS is $\sigma_{PDMS} = 4E^{-13}$ S/m. Considering an applied electric field of 25 MV/m, it follows that the electric field $E_{NF} = 0.023$ MV/m, which is negligible with respect to the applied electric field. As a consequence, the contribution of the electric polarization is disregarded in this study, and, therefore, the additional electrostrictive strain of Equation (15) is not considered for the evaluation of the total stress.

4.3. Equivalent mechanical model of the composite active layer

In this Section, the mechanical model of the active layer of the soft actuator, made of P(VDF-TrFE-CTFE)-based nanofibers integrated in PDMS, is presented.

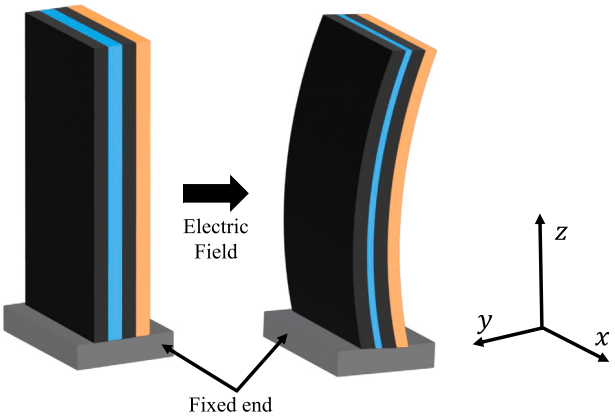

Fig. 9. Working principle of the soft actuator. The actuator composed by the composite layer (blue), surrounded by the carbon black-based electrodes (black), and held by the passive layer (orange), bends when an electric field is applied.

Fig. 9 shows the bending of the soft actuator when an electric field is applied. The figure highlights that a strain is produced due to the Maxwell stress (i.e., the electrodes are attracted to each other and, as a consequence, the active layer is mechanically compressed along the y-axis and expands in the xz-plane). The passive layer resists the deformation, resulting into the bending of the actuator. When the fibers are aligned transversally to the actuator length (i.e., along the x-axis, shown in Fig. 10a), the anisotropy of the active layer given by the higher Young modulus in the fiber direction, enhances the bending of the actuator. Therefore, the actuators with the nanofibers aligned along the x-axis deflect more than the specimen with the nanofibers aligned longitudinally to the actuator length (i.e., along the z-axis, shown in Fig. 10b).

In the case of fibers transversally aligned to the actuator length (Fig. 10a), the composite layer is isotropic in the plane perpendicular to the direction of the nanofibers, i.e., the yz-plane. The strain-stress relation is given by:

$$\begin{bmatrix} \eta_{xx} \\ \eta_{yy} \\ \eta_{zz} \\ 2\eta_{xz} \\ 2\eta_{yz} \\ 2\eta_{xy} \end{bmatrix} = \underbrace{\begin{bmatrix} \frac{1}{Y_z} & -\frac{\mu_{xz}}{Y_x} & -\frac{\mu_{xz}}{Y_x} & 0 & 0 & 0 \\ -\frac{\mu_{xy}}{Y_x} & \frac{1}{Y_x} & -\frac{\mu_{xy}}{Y_x} & 0 & 0 & 0 \\ -\frac{\mu_{xz}}{Y_x} & -\frac{\mu_{xy}}{Y_x} & \frac{1}{Y_x} & 0 & 0 & 0 \\ 0 & 0 & 0 & \frac{2(1+\mu_{xy})}{Y_x} & 0 & 0 \\ 0 & 0 & 0 & 0 & \frac{1}{G_{zx}} & 0 \\ 0 & 0 & 0 & 0 & 0 & \frac{1}{G_{zx}} \end{bmatrix}}_{\kappa_{ij}} \begin{bmatrix} \sigma_{xx} \\ \sigma_{yy} \\ \sigma_{zz} \\ \sigma_{xz} \\ \sigma_{yz} \\ \sigma_{xy} \end{bmatrix} \tag{27}$$

where η and σ represent the strain and stress vectors, respectively, while κ_{ij} is the compliance matrix. The stiffness matrix $\kappa_{ij}^{-1} = C_{ij}$ (κ_{ij} for the scenario of Fig. 10b would have the unit element rotated of 90° around the y-axis) requires the identification of five independent constants:

- Y_z: the Young's modulus in the longitudinal direction of the fibers (z-axis).
- $Y_x = Y_y$: the Young's modulus in the transverse direction of the fibers (x- and y-axis).
- μ_{xz}: the in-plane Poisson's ratio (xz-plane).
- μ_{xy}: the out-of-plane Poisson's ratio (xy-plane).
- G_{zx}: the in-plane shear modulus (xz-plane).

The mechanical properties of the composite material, are obtained experimentally through tensile tests of the integrated nanofibers in PDMS, performed in the Instron™ ElectroPuls E1000 test instrument. The tensile tests have been performed in both the longitudinal and the transversal direction of the fibers to obtain Y_z and $Y_x = Y_y$, respectively.

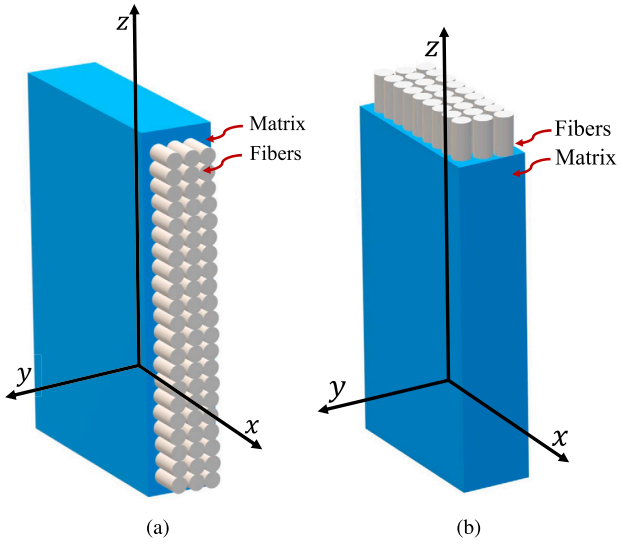

Fig. 10. Composite layer with (a) fibers transversally aligned, i.e., along the x-axis; (b) fibers longitudinally aligned, i.e., along the z-axis.

Table 3
Mechanical parameters of the composite active layer. The average and standard deviation are shown for the experimentally derived values, while the other parameters are evaluated by calculation from the experimental average values.

Y_z [Pa]	$2.2 \cdot 10^7 \pm 3.95 \cdot 10^6$
$Y_x = Y_y$ [Pa]	$4.5 \cdot 10^6 \pm 0.4 \cdot 10^6$
μ_{xz} [-]	0.08 ± 0.019
μ_{xy} [-]	0.39
G_{zx} [Pa]	$2.609 \cdot 10^6$
ρ_c [$\frac{kg}{m^3}$]	792

The in-plane Poisson coefficient μ_{xz} has been evaluated experimentally in a tensile test and by measuring the ratio between the transversal and the longitudinal strain in the material elastic region with the use of a tracking algorithm.

The out-of-plane Poisson coefficient μ_{xy} should be higher than the in-plane Poisson's coefficient which indicates how much the fibers resist a longitudinal deformation with a transverse force [41]. Due to experimental difficulties to evaluate μ_{xy}, the value is initially chosen close to the one of the isotropic PDMS and, then, tuned in the simulation by best fitting with the experimental data.

The out-of-plane shear modulus G_{zx} is given by [42]:

$$G_{zx} = \frac{Y_x}{2(1+\mu_{xz})} \tag{28}$$

The density of the composite ρ_c is given by [43]:

$$\rho_c = (1 - P_{NF})\rho_{NF} + P_{NF}\rho_{PDMS} \tag{29}$$

where P_{NF} is the porosity of the nanofibers, ρ_{NF} and ρ_{PDMS} represent the density of the nanofibers and the PDMS, respectively.

The main mechanical parameters of the composite active layer are summarized in Table 3.

4.4. Dynamic model of the composite soft actuator

The dynamic model of the composite soft actuator is developed by using the finite element modeling software COMSOL Multiphysics® (Burlington, MA, USA, www.comsol.com). Specifically, the electrostrictive module of COMSOL is used for multiphysics simulations that take into account electrostatic (Electrostatics module) and mechanical

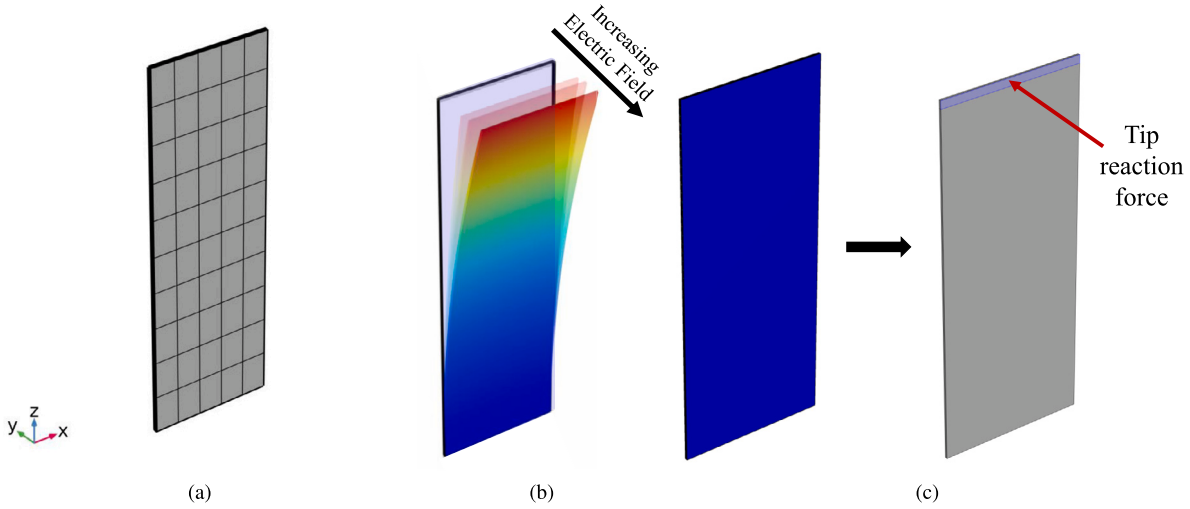

Fig. 11. (a) Mapped mesh of the simulated cantilever beam. (b) Tip deflection simulation, in which the deflection increases for increasing applied electric field. (c) Blocking force simulation, in which the actuator is constrained and the reaction force is evaluated.

physics (Solid Mechanics module). The multiphysics includes the electromechanical force module, that evaluates the Maxwell stress contribution, and the electrostriction module, that evaluates the contribution of the electrical polarization on the actuation.

4.4.1. Solid mechanics COMSOL module

The composite material, surrounded by the flexible electrodes, is built in the simulation environment together with the Kapton® passive layer. The electrodes and the Kapton® passive layer are defined as isotropic elastic materials. The nanofibers integrated in PDMS are considered as a homogeneous elastic anisotropic material, in which the transversally isotropic properties are given by modifying the compliance matrix as shown in Equation (27). The initial values are $u = 0$ (displacement field) and $\partial u/\partial t = 0$ (structural velocity field). The passive and active layers are connected by an union to ensure the continuity of the boundary conditions and a mapped mesh is built (see Fig. 11a).

4.4.2. Electrostatics COMSOL module

For the electrostatics physics, one electrode is set as ground electrode ($V = 0$), while a positive voltage is applied to the other electrode. The initial value is $V = 0$ and, then, charge conservation and zero charge are applied. The composite relative permittivity is defined in the material properties.

4.4.3. Multiphysics COMSOL module

The multiphysics consists of the electromechanical force module, where Equation (13) is computed, and the electrostriction module, which evaluate the additional electrostrictive strain of Equation (15). However, the electrostriction module is disabled for the simulation, since the contribution of the polarization has been disregarded.

The boundary conditions are chosen to be as close as possible to the experimental conditions and, therefore, two different simulations are performed: (i) For the tip deflection test, the structure is mechanically clamped at one end with a fixed constraint, while the other part of the cantilever is free to bend and the deflection is evaluated (Fig. 11b); (ii) For the blocking force test, the structure is mechanically clamped at one hand and a fixed constraint is placed to recreate the actuator tip constrained by the load cell in the experiment. The net reaction force generated at the nodes on the tip surface of the actuator is summed up to obtain the generated blocking force by a surface integration (Fig. 11c).

In case of the actuators where the active layer is composed by longitudinally aligned nanofibers integrated in PDMS, the evaluation method of the blocking force is modified in the model. In fact, as shown in the experiments in Fig. 12, the higher Young's modulus in the fibers direction enhances the lateral extension of the actuator, resulting in a curved tip that touches the load cell with its corners. Therefore, the tip reaction force is evaluated only in the actuator corners in the simulations.

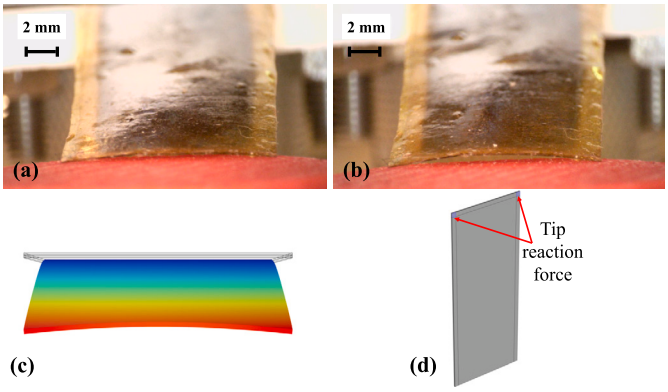

Fig. 12. (a) Actuator tip with no applied electric field. (b) Actuator tip when an electric field of $20 MV/m$ is applied. (c) Simulated tip deflection for longitudinally aligned nanofibers. (d) Evaluation of the tip reaction force for actuators with fiber longitudinally aligned.

The simulations are performed in both steady-state and in the time-transient case. The solver settings for the time dependent solver of the electrostrictive model are set as follow: fully coupled, direct solver, linear system solver MUMPS, free time stepping.

5. Results

This Section presents the results of the electromechanical characterization. Firstly, the experimental data are compared with the physics-based model in steady state and, secondly, the simulation is extended to time-transient and compared with experimental data in the time-domain.

5.1. Steady-state analysis

In this Section, the results of the electromechanical characterization for the actuators fabricated with three different active layers (nanofibers transversally aligned, nanofibers longitudinally aligned, only PDMS) are shown in terms of tip deflection and blocking force.

The experimental data are then compared with the simulation results of the steady-state model, for which the relative permittivity is

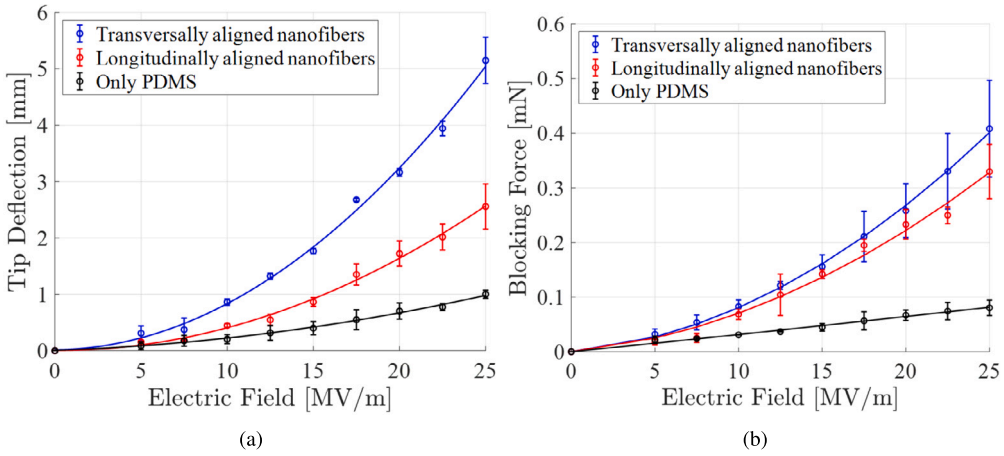

Fig. 13. Electromechanical characterization (mean on at least three specimens and standard deviation) of the soft actuators with transversally aligned nanofibers (blue) longitudinally aligned nanofibers (red) and isotropic pure PDMS (black). (a) Tip deflection. (b) Blocking force.

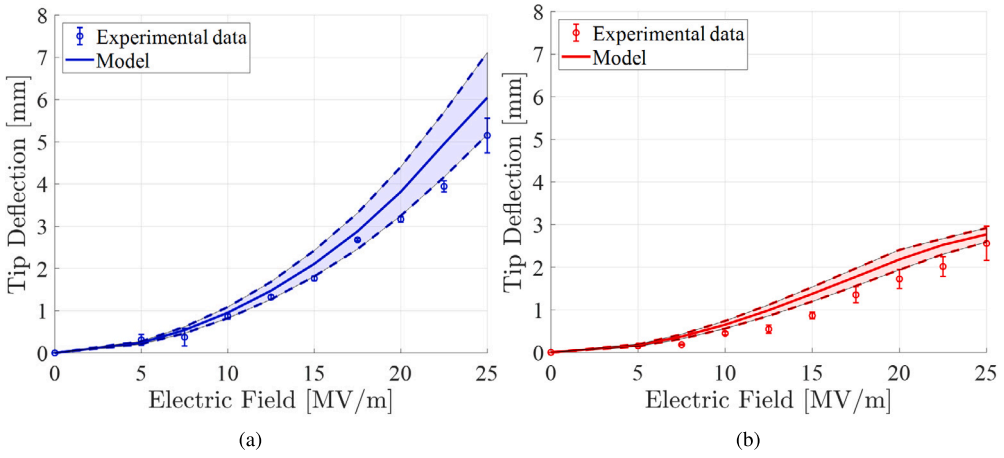

Fig. 14. Experimental and model tip deflections for (a) transversally aligned nanofibers integrated in PDMS (b) longitudinally aligned nanofibers integrated in PDMS. The shaded areas represent the simulation results with the relative permittivity values spanned between 9 and 12.

swept on the basis of the experimental values (average ± standard deviation).

Even though the relative permittivity decreases when the frequency increases as shown in Fig. 7, it is noted that the actuators produce the same tip deflection/blocking forces under DC electric fields and AC electric fields with frequencies below 0.2 Hz [5]. Therefore, the actuators are stimulated either with DC electric fields or with AC electric fields below 0.2 Hz, and the maximum tip deflection/blocking forces are measured.

The measurements are performed on at least three specimens of each type of active layer by stimulating them at different magnitudes of the electric field, ranging from 5 to 25 MV/m. The average value and standard deviation of the maximum tip deflection/blocking force are then calculated for each electric field value. Fig. 13 shows the results of the electromechanical characterization. The experimental data can be fitted by a quadratic interpolation, as expected from the quadratic relationship between the Maxwell stress and the applied electric field. From the Figure, it can be noted that the values of the tip deflections and blocking forces are, as expected, higher for the integrated nanofibers compared to the only PDMS layer. This is due to the higher permittivity and to the anisotropic properties of the composite active layers, as expected from the analysis of Section 4.1. Moreover, it can be noted that the values of the tip deflection/blocking force are further enhanced in the case of transversally aligned fibers. Specifically, compared to the only PDMS at an applied electric field of 25 MV/m, the tip deflection is enhanced of 415% and 150% for transversally and longitudinally aligned nanofibers, respectively, while the blocking force is 400% higher for transversally aligned nanofibers and 300% higher for longitudinally aligned nanofibers.

The experimental results of the electromechanical characterization are compared with the results of the model simulations for the tip deflection in Fig. 14, and for the blocking force in Fig. 15. In the figures, the shaded areas represent the simulation of the model, with the value of the relative permittivity spanning between 9 and 12 (corresponding to the maximum and minimum simulated tip deflection/blocking force in dashed lines), while the continuous lines represent the average measured value of the relative permittivity. Specifically, the minimum and maximum values of the permittivity used in the simulation correspond to the experimental standard deviation obtained in the experimental measurement of the relative permittivity ($\epsilon = 10.5 \pm 1.5$). It can be noted that there is a good match between the experimental data and the simulated model. However, in some cases the simulation slightly overestimates the values measured experimentally. This can be due to the resistivity of the carbon-based soft electrodes (~0.044 Ω/m), and, consequently, to a lower electric field applied during the electromechanical characterization.

5.2. *Time-transient analysis*

As shown by both the experimental measurements and the model simulations, the soft actuator with transversally aligned nanofibers produces higher tip deflections and blocking forces. Therefore, for this

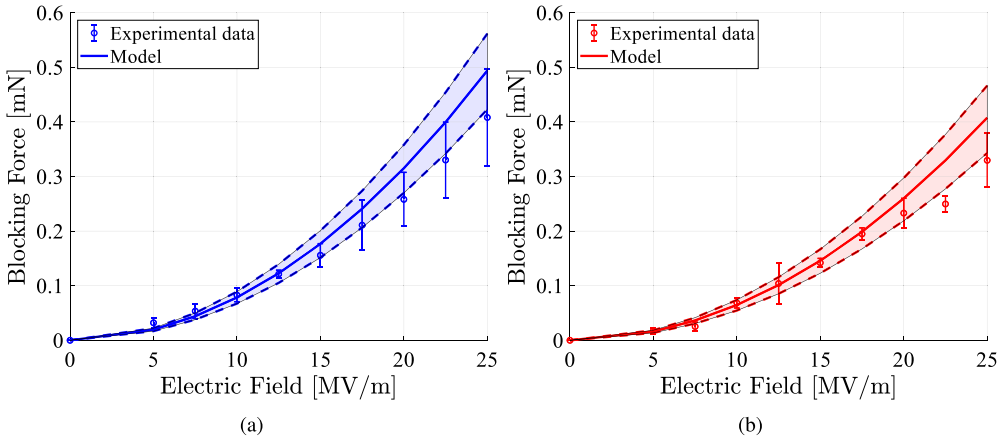

Fig. 15. Experimental and model blocking forces for (a) transversally aligned nanofibers integrated in PDMS (b) longitudinally aligned nanofibers integrated in PDMS. The shaded areas represent the simulation results with the relative permittivity values spanned between 9 and 12.

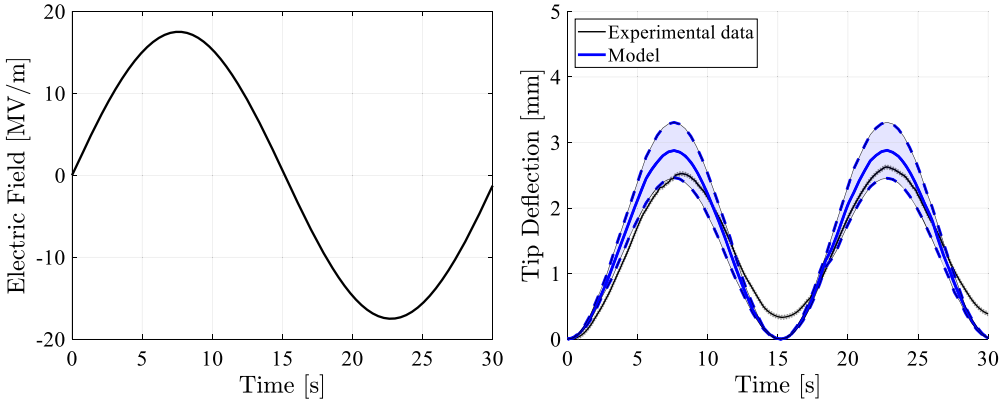

Fig. 16. Time transient experimental data and model tip deflection when a sinusoidal electric field input is applied to (at least) three soft actuators with transversally aligned nanofibers integrated in PDMS. The blue shaded areas represent the simulation results with the relative permittivity values spanned between 9 and 12, while the gray shaded areas represent the standard deviation on the electromechanical characterization.

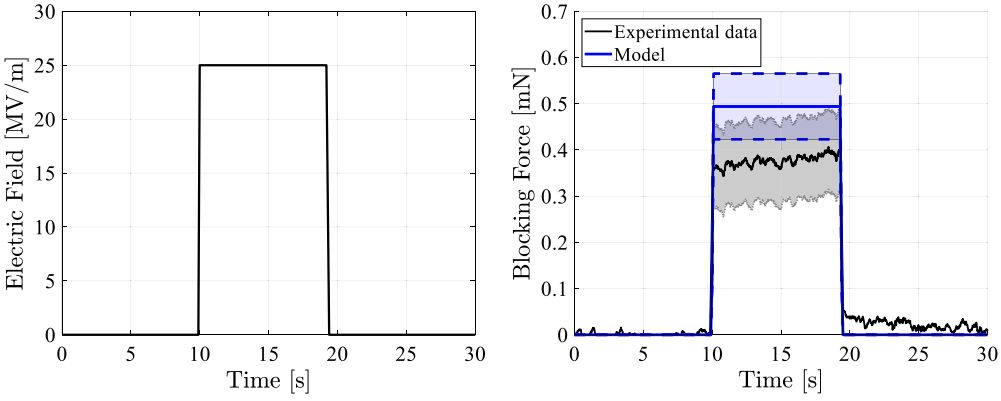

Fig. 17. Time transient experimental and model blocking force when a square electric field input is applied to (at least) three soft actuators with transversally aligned nanofibers integrated in PDMS. The blue shaded areas represent the simulation results with the relative permittivity values spanned between 9 and 12, while the gray shaded areas represent the standard deviation on the electromechanical characterization.

configuration, a time-transient simulation is performed to compare the model with the experimental data. Fig. 16 shows the tip deflection and Fig. 17 the blocking force, when two different time-dependent electric field inputs are considered.

As for the steady-state case, the shaded areas represent the simulation results with the relative permittivity values spanned between 9 and 12 (corresponding to the maximum and minimum simulated tip deflection/blocking force in dashed lines). The experimental data are represented in black, where the means are plotted with continuous lines while the standard deviations with dashed lines. As it can be noted from Fig. 16, the tip deflection is independent from the polarity of the electric field due to the quadratic relation between the stress and the applied electric field.

It is possible to notice that the model, which has been build considering a pure elastic material, does not catch the viscous nature of this electrostrictive actuator which is characterized by a nonlinear viscoelas-

tic behavior, i.e., the tip deflection/blocking force responses consist of a nonlinear instantaneous elastic response and a slower viscous response [25]. Specifically, the actuators exhibit creep behavior, which means that the actuator continues to bend after the electric field has reached a steady level, and a viscoelastic relaxation, which consist in a non linear stress relaxation when the applied electric field is equal to zero. Since the material is viscoelastic, the components of the stiffness matrix C_{ij} (Equation (27) in Section 4.3) should be a function of time [44]. Therefore, the viscoelasticity of the material has to be added in the simulation parameters.

The viscoelastic behavior of a polymer can be described by a generalized Maxwell model [45,46], given by the parallel of n branches containing the series of a spring and a damper, as shown in Fig. 18, where Y_0 represents the long-term stiffness derived from the elastic part, while $Y_1, \cdots, Y_n$ represent the stiffness in the n branches, $\mu_1, \cdots, \mu_n$ are the viscosity coefficients in the n branches, and σ is the stress applied to the polymer.

The COMSOL viscoelastic subnode is added to insert the viscous stress contribution to the elastic material. Specifically, a generalized Maxwell model with one branch ($n = 1$) is used in this study. The subnode requires to insert two viscoelastic parameters that are the stiffness in the viscoelastic branch and the relaxation time. The classical relaxation curve can be described using the generalized Maxwell model as:

$$\sigma(t) = \sigma_0 e^{-t/\tau} \tag{30}$$

where σ_0 is the initial stress at the initial time t_0, and τ is the relaxation time defined by:

$$\tau = \frac{\mu_1}{Y_1} \tag{31}$$

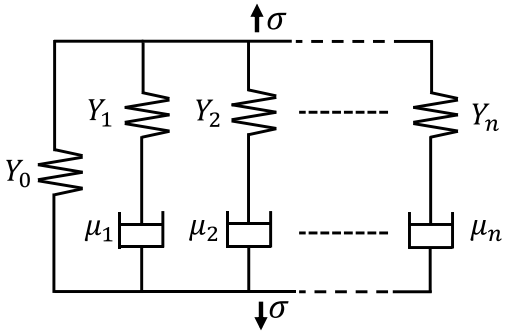

Fig. 18. Schematic of the generalized Maxwell model for viscoelastic materials [45,46].

The response time of the actuator is determined by both the time needed for the deformation of the polymer (determined by its viscoelastic property), and the time constant of the equivalent RC circuit, as shown in Fig. 6.

The viscoelastic parameters are, typically, determined with mechanical creep experiments. However, a uniform stress can be achieved by applying a step-electric field input [47]. In this way, the delay given by the electrical time constant of the RC circuit is also taken into account.

Square electric field inputs have been applied to the actuator. The resulting blocking force is measured and the relaxation curve is fitted by using Equation (30), as shown in Fig. 19a. A relaxation time of $\tau = 0.5 \pm 0.2$ has been obtained.

The stiffness in the viscoelastic branch is evaluated with a dynamic mechanical analysis tensile test. Three specimens of the soft actuators with nanofibers integrated in PDMS are subjected to dynamic sinusoidal strains at varying frequencies, and the sinusoidal stress response is recorded. During the test, the storage modulus is evaluated by a linear interpolation of the dynamic stress-strain loops at different frequency values. The dependency between the modulus and frequency is reported in Fig. 19b.

The dependency between the complex modulus and the frequency is inserted in the viscoelastic parameters of the FEM simulation as a cubic spline interpolation of the experimental data.

The instantaneous modulus Y_0 is defined as the long-term modulus plus the sum of the stiffness of the viscoelasticity branch, i.e.:

$$Y_0 = Y + Y_n \tag{32}$$

which represents the equivalent stiffness when the load is applied much faster then the relaxation time of the viscoelastic branch.

The stress tensor σ, given by Equation (14), is augmented by the viscoelastic stress derived from Y_n. The electromechanical characterization is compared with the results of the model with the addition of viscoelastic properties for the tip deflection (see Fig. 20) and blocking force (see Fig. 21). From the figures, it is possible to notice that both creep and relaxation behavior have been now included in the model and are evident in the simulation results.

6. Discussion

This Section aims to delve deeper into the actuator parameters and performances, specifically examining how the amount of porosity exhibited by the P(VDF-TrFE-CTFE) nanofibers influences them. By analyzing this crucial relationship, valuable insights can be uncovered that shed light on the interplay between porosity and the overall actuator behavior.

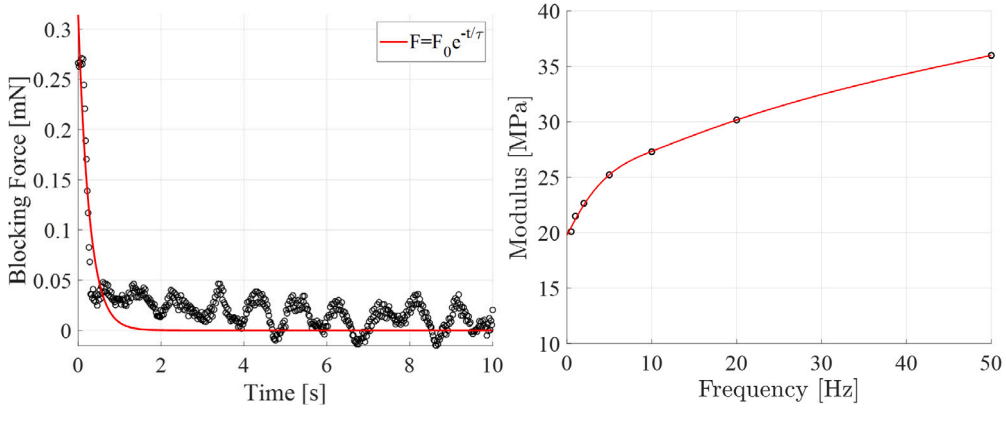

Fig. 19. (a) Fitting of the experimental relaxation curve (black scatter) of a blocking force experiment with the Maxwell exponential relaxation curve and (b) dependency of the complex modulus on the frequency.

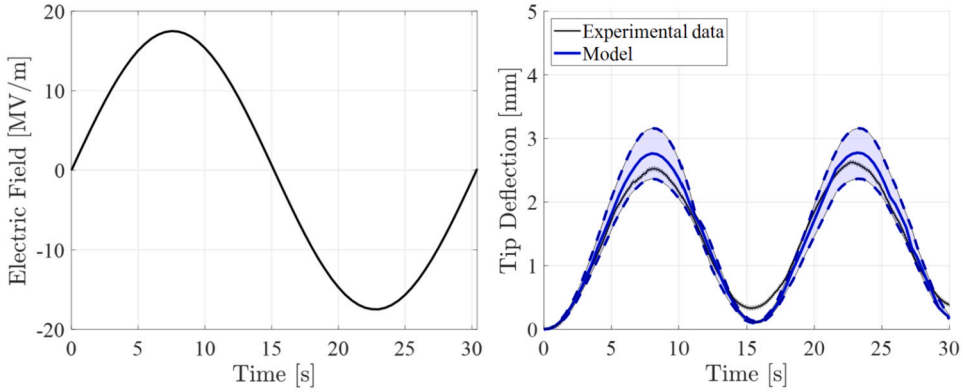

Fig. 20. Time transient experimental and model tip deflection when a sinusoidal electric field input is applied to (at least) three soft actuators with transversally aligned nanofibers integrated in PDMS. The blue shaded areas represent the simulation results with the relative permittivity values spanned between 9 and 12, while the gray shaded areas represent the standard deviation on the electromechanical characterization.

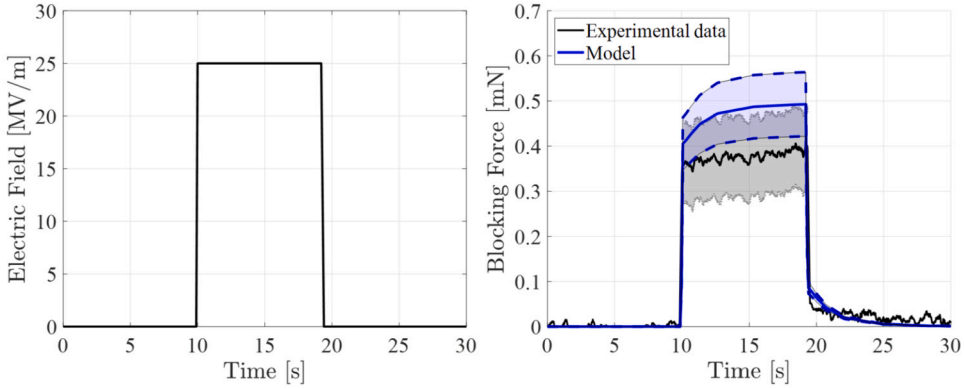

Fig. 21. Time transient experimental and model blocking force when a square electric field input is applied to (at least) three soft actuators with transversally aligned nanofibers integrated in PDMS. The blue shaded areas represent the simulation results with the relative permittivity values spanned between 9 and 12, while the gray shaded areas represent the standard deviation on the electromechanical characterization.

6.1. Nanofibers porosity vs. relative permittivity

In applications that utilize electroactive polymers as actuators, achieving an optimal balance between the strain response and blocking force is of paramount importance. This can be accomplished by increasing the relative permittivity of the polymer, thereby enhancing both aspects simultaneously.

Fig. 22a illustrates the direct proportionality between the porosity of the electrospun nanofibers and the final values of the relative permittivity within the composite material, as predicted by the electrical model (see Equation (19)). The overall relative permittivity of the composite material is determined by a weighted average of the relative permittivity values of its individual components. When the porosity of the nanofibers is decreased, the relative permittivity of the nanofibers, which is higher than that of PDMS, has a stronger influence on the final properties of the composite. As a result, the relative permittivity of the composite material is enhanced. However, it is essential to acknowledge that increasing the relative permittivity may potentially compromise the dielectric breakdown strength of the composite material [48]. Therefore, to improve and to maximize the overall actuator performances in terms of strain response and blocking force, it becomes imperative to strike a harmonious equilibrium among various key parameters, including the relative permittivity, electrical breakdown resistance, and the desired electric field range.

6.2. Nanofibers porosity vs. mechanical properties of the composite layer

The influence of fibers porosity on the mechanical properties of the resulting composite material has been well-documented in [49]. In conventional unidirectional and continuous composites, the prediction of the composite axial Young's modulus and transverse Young's modulus typically follows the established rule-of-mixtures [50], which provides a straightforward means to estimate the values of these moduli by considering the contributions of the constituent materials, enabling researchers to make informed decisions regarding material design and optimization. Specifically, following the notation of Equation (27), the Young's modulus in the fibers direction can be written as:

$$Y_z = Y_{fz} V_f + Y_{PDMS} V_{PDMS} \tag{33}$$

where Y_{fz} represents the Young's modulus of the nanofibers in the alignment direction, Y_{PDMS} represents the PDMS Young's modulus, V_f represents the fibers volume fraction and V_{PDMS} indicates the PDMS volume fraction.

Similarly, the composite modulus in the transverse direction can be written as:

$$Y_x = Y_y = \frac{Y_{fx} V_{PDMS}}{Y_{fx} V_{PDMS} + Y_{PDMS} V_f} \tag{34}$$

where Y_{fx} represents the Young's modulus of the nanofibers in the transverse direction.

The porosity of the nanofibers is directly related to the volume fractions of the individual materials (V_f and V_{PDMS}) in the final composite. Therefore, the amount of porosity significantly affects the mechanical properties of the composite material. Specifically, the orthogonal modulus ratio (the modulus in the fiber direction divided by the one in transversal direction Y_z/Y_x) is an important parameter when designing anisotropic actuators [23]. By increasing the orthogonal modulus, the

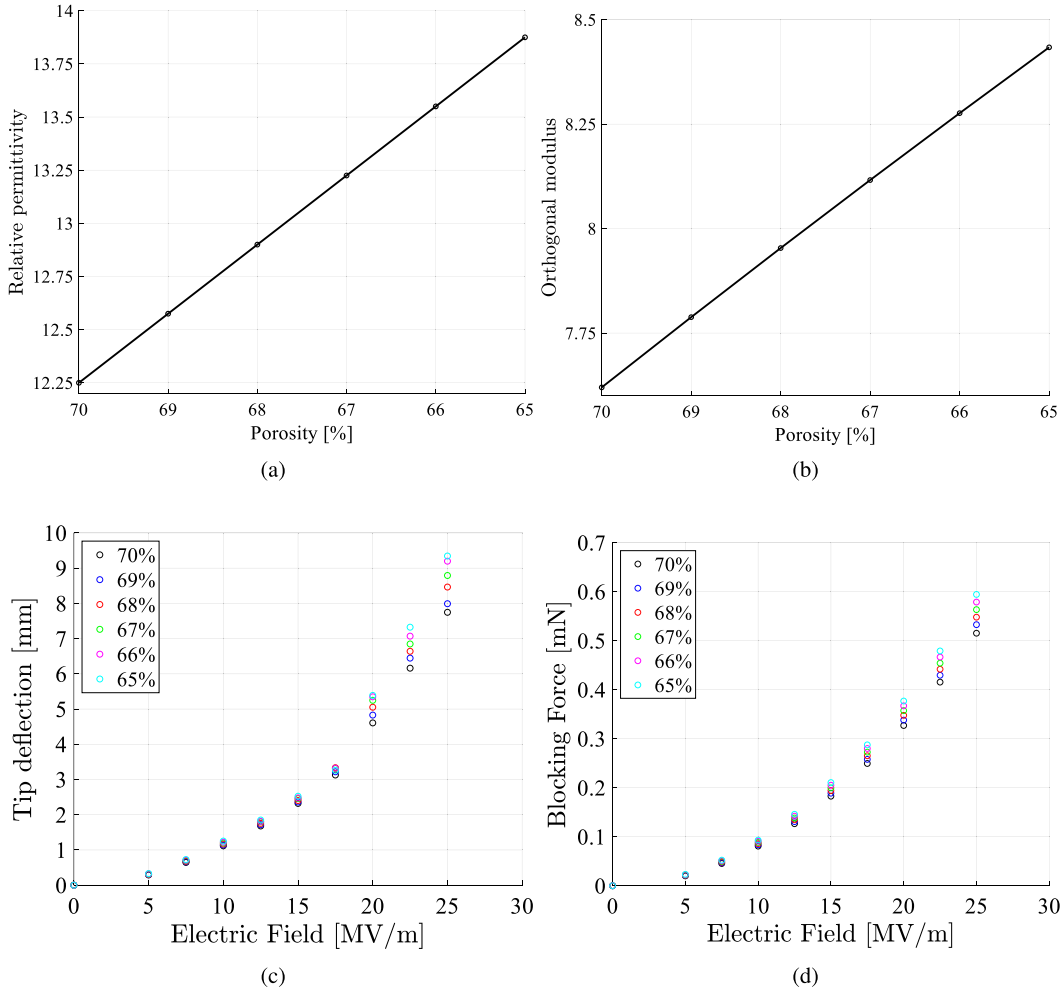

Fig. 22. Influence of the nanofibers porosity on the (a) relative permittivity, (b) orthogonal modulus, (c) blocking force, (d) tip deflection.

anisotropic properties of composite actuators can be enhanced. Fig. 22b shows the direct proportionality between porosity and orthogonal modulus of the integrated nanofibers in PDMS, as follows the rule of mixtures.

6.3. Nanofibers porosity vs. actuators performances

As previously shown, the nanofibers porosity has an influence on both mechanical and electrical properties of the composite active layer. Therefore, by reducing the porosity of the nanofibers, the actuator tip deflection and blocking force, can be enhanced. The realized physics based model (in steady state) is modified by varying the nanofibers porosity and, therefore, proportionally varying the Young moduli and the relative permittivity of the active layer in the model (while keeping the Poisson coefficients constant). With decreasing porosity, the relative permittivity and the orthogonal modulus are both enhanced and, consequently, the electromechanical properties of the actuator are improved, as depicted in Fig. 22c for the tip deflection and Fig. 22d for the blocking force, for the case of an actuator with transversely aligned nanofibers.

With decreasing porosity, the relative permittivity and the orthogonal modulus are simultaneously enhanced as well as the electromechanical properties of the actuator, as predicted by the model. However, the rule of mixtures provides only an estimation of the composite properties. Therefore, further experimental investigation is needed to evaluate the influence of the electrospun nanofibers porosity on the electromechanical properties of the actuator.

6.4. Future work

The relative permittivity and the orthogonal modulus are the main parameters needed to increase the actuators performances. Therefore, future work will be directed toward augmenting these specific parameters. It has been previously demonstrated that the alteration of porosity plays a direct and influential role in modulating these parameters.

The porosity can be tuned by directly manipulating the electrospinning parameters. Factors such as flow rate, applied voltage, utilized solvents, needle gauge, and the distance between the jet evolution point and the deposition point exert significant influence over crucial characteristics such as fiber diameter, density, and the porosity. This ability to control and fine-tune porosity, also with the help of predictive models [51], can be used to precisely tailor the desired properties of the electrospun nanofibers and, ultimately, of the nanofibrous soft actuators.

By following the constitutive model of the actuator, also changing the integration matrix would influence both the Young's modulus (according to mixture theory) and the relative permittivity, as suggested by the relative permittivity model. Using high permittivity PDMS mixtures [52–54] or varying its Young modulus [55], may enhance the electromechanical coupling and, consequently, the actuation.

Nevertheless, the choice of material for an electrostrictive actuator involves a trade-off between key parameters, such as actuation performances, stiffness, relative permittivity and electrical breakdown resistance, which are influenced by the matrix selected for the integration of the nanofibers.

7. Conclusion

This study analyzed P(VDF-TrFE-CTFE)-based aligned electrospun nanofibers immersed into a PDMS matrix. The composite material, obtained by the integration of the nanofibers into the PDMS through a designed blading process, is used as active layer of a unimorph cantilever beam soft actuator. The composite active layer is electrically and mechanically modeled and a physics-based model, using finite element analysis, is realized to describe the actuator behavior. The actuator is electromechanically characterized, to analyze and measure the tip deflection and the blocking force, showing an intrinsically anisotropic behavior of the actuator due to the alignment of the nanofibers in the PDMS matrix. Thanks to the increased relative permittivity and to the anisotropic properties, the actuators with integrated nanofibers show higher tip deflection and blocking force, compared to the pure PDMS. The actuation is further enhanced by transversally aligning the nanofibers to the length of the actuator in the PDMS matrix, exploiting the mechanical anisotropic properties of the aligned nanofibers.

The model is validated with the experimental results obtained from the electromechanical characterization, showing a good match between the simulated and the experimental values for both steady state and time transient simulations. Moreover, the effect of the nanofibers porosity on the actuator electromechanical properties is studied thanks to the realized model.

The electromechanical properties of the proposed soft actuator, as showed in the experimental characterization and further analyzed thanks to the physics-based model, demonstrate the possibility of using electrospun nanofibers of P(VDF-TrFE-CTFE) integrated in PDMS as soft actuator.

Declaration of competing interest

The authors declare that they have no known competing financial interests or personal relationships that could have appeared to influence the work reported in this paper.

Data availability

Data will be made available on request.

Acknowledgements

This work was funded by the European Commission's Horizon 2020 Programme as part of the project MAGNIFY under grant no. 801378.

The SEM images were taken at the Microscopy and Imaging Center (UMIC) of the University Medical Center Groningen (The Netherlands) sponsored by ZonMw grant 91111.006 (Zeiss Supra55 ATLAS).

The authors would like to thank Niklas Erdmann and Daniela Metello (MSc students at the Robotics Lab, Bernoulli Institute for Mathematics, Computer Science and Artificial Intelligence, Faculty of Science and Engineering, University of Groningen, The Netherlands) for their help during the fabrication and electro-mechanical characterization of the soft actuators.

References

[1] N. Della Schiava, M.-Q. Le, J. Galineau, F. Domingues Dos Santos, P.-J. Cottinet, J.-F. Capsal, Influence of plasticizers on the electromechanical behavior of a P(VDF-TrFE-CTFE) terpolymer: toward a high performance of electrostrictive blends, J. Polym. Sci., Part B, Polym. Phys. 55 (4) (2017) 355–369.

[2] P. Lheritier, S. Noel, N. Vaxelaire, F.D. Dos Santos, E. Defay, Actuation efficiency of polyvinylidene fluoride-based co- and ter-polymers, Polymer 156 (2018) 270–275.

[3] C. Gotti, A. Sensini, A. Zucchelli, R. Carloni, M.L. Focarete, Hierarchical fibrous structures for muscle-inspired soft-actuators: a review, Appl. Mater. Today 20 (2020) 100772.

[4] R. D'Anniballe, N. Erdmann, G. Selleri, R. Carloni, Dynamic modeling of P(VDF-TrFE-CTFE)-based soft actuators via echo state networks, in: IEEE/ASME International Conference on Advanced Intelligent Mechatronics, 2022, pp. 118–124.

[5] R. D'Anniballe, A. Zucchelli, R. Carloni, The effect of morphology on poly (vinylidene fluoride-trifluoroethylene-chlorotrifluoroethylene)-based soft actuators: films and electrospun aligned nanofiber mats, Sens. Actuators A, Phys. (2021) 113255.

[6] G. Selleri, F. Mongiolì, E. Maccaferri, R. D'Anniballe, L. Mazzocchetti, R. Carloni, D. Fabiani, A. Zucchelli, T.M. Brugo, Self-sensing soft skin based on piezoelectric nanofibers, Polymers 15 (2) (2023) 280.

[7] G. Selleri, M.E. Gino, T.M. Brugo, R. D'Anniballe, J. Tabucol, M.L. Focarete, R. Carloni, D. Fabiani, A. Zucchelli, Self-sensing composite material based on piezoelectric nanofibers, Mater. Des. 219 (2022) 110787.

[8] J. He, X. Guo, J. Yu, S. Qian, X. Hou, M. Cui, Y. Yang, J. Mu, W. Geng, X. Chou, A high-resolution flexible sensor array based on PZT nanofibers, Nanotechnology 31 (15) (2020) 155503.

[9] D. Chen, R. Wang, W.W. Tjiu, T. Liu, High performance polyimide composite films prepared by homogeneity reinforcement of electrospun nanofibers, Compos. Sci. Technol. 71 (13) (2011) 1556–1562.

[10] L. Liu, Y. Zhou, S. Pan, Experimental and analysis of the mechanical behaviors of multi-walled nanotubes/polyurethane nanoweb-reinforced epoxy composites, J. Reinf. Plast. Compos. 32 (11) (2013) 823–834.

[11] A. Kausar, Mechanical, thermal, and electrical properties of epoxy matrix composites reinforced with polyamide-grafted-MWCNT/poly(azo-pyridine-benzophenone-imide)/polyaniline nanofibers, Int. J. Polym. Mater. Polym. Biomater. 63 (16) (2014) 831–839.

[12] H.-R. Jung, D.-H. Ju, W.-J. Lee, X. Zhang, R. Kotek, Electrospun hydrophilic fumed silica/polyacrylonitrile nanofiber-based composite electrolyte membranes, Electrochim. Acta 54 (13) (2009) 3630–3637.

[13] L. Ji, Z. Lin, R. Zhou, Q. Shi, O. Toprakci, A.J. Medford, C.R. Millns, X. Zhang, Formation and electrochemical performance of copper/carbon composite nanofibers, Electrochim. Acta 55 (5) (2010) 1605–1611.

[14] L. Ji, Y. Yao, O. Toprakci, Z. Lin, Y. Liang, Q. Shi, A.J. Medford, C.R. Millns, X. Zhang, Fabrication of carbon nanofiber-driven electrodes from electrospun polyacrylonitrile/polypyrrole bicomponents for high-performance rechargeable lithium-ion batteries, J. Power Sources 195 (7) (2010) 2050–2056.

[15] B. Qiao, X. Wang, S. Tan, W. Zhu, Z. Zhang, Synergistic effects of Maxwell stress and electrostriction in electromechanical properties of poly(vinylidene fluoride)-based ferroelectric polymers, Macromolecules 52 (22) (2019).

[16] R. Hinchet, H. Shea, High force density textile electrostatic clutch, Adv. Mater. Technol. 5 (4) (2020) 1900895.

[17] D. Wu, Q. Zhou, K.K. Shung, S.N. Bharadwaja, D. Zhang, H. Zheng, Dielectric and piezoelectric properties of PZT composite thick films with variable solution to powder ratios, J. Am. Ceram. Soc. 92 (6) (2009) 1276–1279.

[18] H. Kueppers, T. Leuerer, U. Schnakenberg, W. Mokwa, M. Hoffmann, T. Schneller, U. Boettger, R. Waser, PZT thin films for piezoelectric microactuator applications, Sens. Actuators A, Phys. 97 (2002) 680–684.

[19] T. Jow, P. Cygan, Dielectric breakdown of polyvinylidene fluoride and its comparisons with other polymers, J. Appl. Phys. 73 (10) (1993) 5147–5151.

[20] J. Chen, X. Xiong, L. Shui, Q. Zhang, H. Yang, F. Zhang, Enhanced dielectric constant and hydrophobicity of P(VDF-TrFE)-based composites, J. Mater. Sci., Mater. Electron. 29 (20) (2018) 17612–17621.

[21] J.-H. Bae, S.-H. Chang, Characterization of an electroactive polymer (PVDF-TrFE) film-type sensor for health monitoring of composite structures, Compos. Struct. 131 (2015) 1090–1098.

[22] H. Qin, T. Zhang, N. Li, H.-P. Cong, S.-H. Yu, Anisotropic and self-healing hydrogels with multi-responsive actuating capability, Nat. Commun. 10 (1) (2019) 2202.

[23] J. He, Z. Chen, Y. Xiao, X. Cao, J. Mao, J. Zhao, X. Gao, T. Li, Y. Luo, Intrinsically anisotropic dielectric elastomer fiber actuators, ACS Mater. Lett. 4 (3) (2022) 472–479.

[24] Y. Wang, N. Wu, C. Liu, M.K. Albolkany, M. Wang, Y. Wang, S. Arooj, W. Zhang, B. Liu, Stimuli-responsive anisotropic actuation of melem-formaldehyde polymer, Mater. Horiz. 7 (1) (2020) 149–156.

[25] R. Carloni, V.I. Lapp, A. Cremonese, J. Belcari, A. Zucchelli, A variable stiffness joint with electrospun P(VDF-TrFE-CTFE) variable stiffness springs, IEEE Robot. Autom. Lett. 3 (2) (2018) 973–978.

[26] A. Sensini, C. Gualandi, L. Cristofolini, G. Tozzi, M. Dicarlo, G. Teti, M. Mattioli-Belmonte, M.L. Focarete, Biofabrication of bundles of poly (lactic acid)-collagen blends mimicking the fascicles of the human Achille tendon, Biofabrication 9 (1) (2017) 015025.

[27] G. Selleri, D. Fabiani, A. Zucchelli, T.M. Brugo, F. Grolli, L. Bordoni, Development of flexible sensors based on piezoelectric nanofibers, in: IEEE International Conference on the Properties and Applications of Dielectric Material, 2021, pp. 358–361.

[28] R. D'Anniballe, G. Paoletta, R. Carloni, A polyurethane-based electrospun nanofiber bundle soft actuator: fabrication, modeling, and control, in: IEEE International Conference on Soft Robotics, IEEE, 2021, pp. 393–398.

[29] C. Maruccio, L. De Lorenzis, L. Persano, D. Pisignano, Computational homogenization of fibrous piezoelectric materials, Comput. Mech. 55 (2015) 983–998.

[30] Y. Yin, D. Zhao, J. Liu, Z. Xu, Nonlinear dynamic analysis of dielectric elastomer membrane with electrostriction, Appl. Math. Mech. 43 (6) (2022) 793–812.

[31] A. Ask, A. Menzel, M. Ristinmaa, Modelling of viscoelastic dielectric elastomers with deformation dependent electric properties, Proc. IUTAM 12 (2015) 134–144.

[32] K. Jia, T. Lu, Numerical study on the electromechanical behavior of dielectric elastomer with the influence of surrounding medium, Int. J. Smart Nano Mater. 7 (1) (2016) 52–68.

[33] A. Dorfmann, R. Ogden, Nonlinear electroelasticity, Acta Mech. 174 (3–4) (2005) 167–183.
[34] J.A. Stratton, Electromagnetic Theory, vol. 33, John Wiley & Sons, 2007.
[35] F. Li, L. Jin, Z. Xu, S. Zhang, Electrostrictive effect in ferroelectrics: an alternative approach to improve piezoelectricity, Appl. Phys. Rev. 1 (1) (2014) 011103.
[36] Y. Shkel, Electrostriction: material parameters and stress/strain constitutive relations, Philos. Mag. 87 (11) (2007) 1743–1767.
[37] F.M. Guillot, J. Jarzynski, E. Balizer, Measurement of electrostrictive coefficients of polymer films, J. Acoust. Soc. Am. 110 (6) (2001) 2980–2990.
[38] C.L. Hom, N. Shankar, A finite element method for electrostrictive ceramic devices, Int. J. Solids Struct. 33 (12) (1996) 1757–1779.
[39] P. Sarafis, A.G. Nassiopoulou, Dielectric properties of porous silicon for use as a substrate for the on-chip integration of millimeter-wave devices in the frequency range 140 to 210 GHz, Nanoscale Res. Lett. 9 (1) (2014) 1–8.
[40] B. Isaac, R.M. Taylor, K. Reifsnider, Anisotropic characterizations of electrospun pan nanofiber mats using design of experiments, Nanomaterials 10 (11) (2020) 2273.
[41] A.G. Adeniyi, S.A. Adeoye, D.V. Onifade, J.O. Ighalo, Multi-scale finite element analysis of effective elastic property of sisal fiber-reinforced polystyrene composites, Mech. Adv. Mat. Struct. 28 (12) (2021) 1245–1253.
[42] V.L. Popov, M. Heß, E. Willert, Handbook of Contact Mechanics: Exact Solutions of Axisymmetric Contact Problems, Springer Nature, 2019.
[43] M. Ashby, Selecting the components of composites, J. Phys. IV 3 (C7) (1993) C7-1595.
[44] D. Morris, H. Brinson, Y. Yeow, The viscoelastic behavior of the principal compliance matrix of a unidirectional graphite/epoxy composite, Polym. Compos. 1 (1) (1980) 32–36.
[45] T. Nguyen, J. Li, L. Sun, D. Tran, F. Xuan, Viscoelasticity modeling of dielectric elastomers by Kelvin Voigt-generalized Maxwell model, Polymers 13 (13) (2021) 2203.
[46] S. Adamczak, J. Bochnia, Estimating the approximation uncertainty for digital materials subjected to stress relaxation tests, Metrol. Meas. Syst. 23 (4) (2016) 545–553.
[47] R. Sarban, B. Lassen, M. Willatzen, Dynamic electromechanical modeling of dielectric elastomer actuators with metallic electrodes, IEEE/ASME Trans. Mechatron. 17 (5) (2011) 960–967.
[48] N. Della Schiava, K. Thetpraphi, M.-Q. Le, P. Lermusiaux, A. Millon, J.-F. Capsal, P.-J. Cottinet, Enhanced figures of merit for a high-performing actuator in electrostrictive materials, Polymers 10 (3) (2018) 263.
[49] B. Madsen, H. Lilholt, Physical and mechanical properties of unidirectional plant fibre composites — an evaluation of the influence of porosity, Compos. Sci. Technol. 63 (9) (2003) 1265–1272.
[50] T.W. Clyne, D. Hull, An Introduction to Composite Materials, Cambridge University Press, 2019.
[51] T. Wang, W. Dong, Y. Chen, T. Pan, R. Chen, Study on porosity of electrospun nanofiber membrane by neural network, Appl. Math. Sci. 12 (2018) 1059–1074.
[52] W. Wang, G. Ren, M. Zhou, W. Deng, Preparation and characterization of CCTO/PDMS dielectric elastomers with high dielectric constant and low dielectric loss, Polymers 13 (7) (2021) 1075.
[53] M. Tian, Z. Wei, X. Zan, L. Zhang, J. Zhang, Q. Ma, N. Ning, T. Nishi, Thermally expanded graphene nanoplates/polydimethylsiloxane composites with high dielectric constant, low dielectric loss and improved actuated strain, Compos. Sci. Technol. 99 (2014) 37–44.
[54] G. Liu, Y. Chen, M. Gong, X. Liu, Z.-K. Cui, Q. Pei, J. Gu, C. Huang, Q. Zhuang, Enhanced dielectric performance of PDMS-based three-phase percolative nanocomposite films incorporating a high dielectric constant ceramic and conductive multi-walled carbon nanotubes, J. Mater. Chem. C 6 (40) (2018) 10829–10837.
[55] R. Seghir, S. Arscott, Extended PDMS stiffness range for flexible systems, Sens. Actuators A, Phys. 230 (2015) 33–39.